Engineering Structures 359 (2026) 122666

Contents lists available at ScienceDirect

Engineering Structures

journal homepage: www.elsevier.com/locate/engstruct

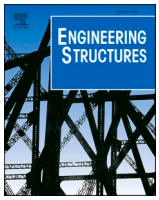

Towards improved normative definitions of damping in railway bridges: Insights from the InBridge4EU European experimental database

P.A. Montenegro [a,*], E. Laligant [b], F. Pimenta [a], A. Silva [a], O. Ahmed [b], C. Laurent [b], A. Andersson [c]

[a] CONSTRUCT, Faculty of Engineering, University of Porto, Rua Dr. Roberto Frias s/n, Porto 4200-465, Portugal
[b] AVLS, Bureau d'Études en Acoustique et Vibrations, 18 Rue Charles de Gaulle, Orsay 91400, France
[c] Division of Structural Engineering and Bridges, KTH Royal Institute of Technology, Stockholm SE-100 44, Sweden

ARTICLE INFO

Keywords:
Bridge damping
Railway bridges
Eurocode
Damping estimation algorithms
InBridge4EU project
Normative guidelines

ABSTRACT

Recent measurement campaigns under the Shift2Rail In2Track2 and In2Track3 projects have shown that damping levels in existing railway bridges often exceed the conservative values prescribed in EN 1991–2. These studies also revealed significant scatter among similar structures, reflecting the complex influence of soil–structure interaction, vibration amplitude, and estimation methods. Given the critical role of damping in bridge dynamics, particularly near resonance, and in light of the challenges outlined above, an update of the Eurocode provisions is needed. In this context, the European Union Agency for Railways (ERA) and Europe's Rail Joint Undertaking (EU-Rail) launched the InBridge4EU project to improve the representation of damping in the Eurocode framework. This paper presents its main outcomes based on over 1150 traffic-induced acceleration records from nearly 90 bridges across five European countries. The analysis resulted in the first proposal since the 1990s for revised damping curves and an updated bridge typology classification that better reflects real-world variability. These results provide a more robust, data-driven basis for the forthcoming revision of EN 1991–2, enabling less conservative yet safe design approaches and contributing to more efficient and reliable dynamic assessment of railway bridges in the European network.

1. Introduction

Determining structural damping in railway bridges remains one of the most challenging aspects of dynamic assessment, as it results from multiple interacting energy dissipation mechanisms within the bridge, track, vehicle, and foundations [1]. Each interface, namely track–bridge, soil–structure, and train–bridge, contributes differently, making reliable estimation particularly complex. At the bridge level, damping depends mainly on material behaviour, although non-structural components such as bearings, joints, and handrails can also play a role [2]. Track–bridge interaction and radiation effects in the soil further influence overall damping and may vary seasonally or with vibration amplitude [3,4].

Because of its complex origins, experimental characterisation of damping is difficult. Common testing methodologies include ambient vibration tests [5,6], tests under railway traffic [6], and forced vibration tests using external excitation [7,8]. Ambient tests are simple but often inadequate to reproduce train-induced responses, whereas the latter two are more representative of in-service dynamic conditions.

Several methods exist for estimating damping, notably the Logarithmic Decrement (LD), Prony–Pisarenko (PP), and stochastic approaches [5,9,10]. The LD method is widely used for single-mode responses, but its reliability decreases when modes interact, such as in bending–torsion coupling. A recent review [11] emphasises that damping values strongly depend on temperature, excitation amplitude, and identification algorithm, highlighting the need for harmonised methodologies and consistent datasets

Damping is particularly relevant near resonance, where dynamic amplification can become critical, especially for high-speed operations [9,12]. Because accurate damping estimates are difficult to obtain, the European Rail Research Institute (ERRI) D214 committee adopted conservative lower-bound values for different bridge families [9], later incorporated into EN 1991–2 [13] and retained in current versions [12]. While these values ensure safety, they can lead to over-conservative

* Corresponding author.
E-mail addresses: paires@fe.up.pt (P.A. Montenegro), etienne.laligant@avls-fr.com (E. Laligant), fnpimenta@fe.up.pt (F. Pimenta), ajpsilva@fe.up.pt (A. Silva), omar.ahmed@avls-fr.com (O. Ahmed), christophe.laurent@avls-fr.com (C. Laurent), andreas.andersson@byv.kth.se (A. Andersson).

https://doi.org/10.1016/j.engstruct.2026.122666
Received 29 October 2025; Received in revised form 15 February 2026; Accepted 1 April 2026
Available online 8 April 2026

dynamic assessments and unnecessary design costs [14].

Since the ERRI D214 report, studies dedicated to railway bridge damping have remained limited. Gattulli *et al.* [15] analysed two Italian bridges using the Stochastic Subspace Identification (SSI) method, Stollwitzer *et al.* [1] investigated energy dissipation modes in ballasted tracks, and Silva *et al.* [10] examined four Portuguese filler-beam bridges using the PP algorithm. More recently, Stollwitzer *et al.* [16, 17] proposed data-driven damping models linking damping with span length and bearing type, stating that EN 1991–2 [12] may underestimate damping by up to 80%. Although these studies revealed the conservatism of EN 1991–2, few proposed clear normative alternatives, nor relied on sufficiently large and representative datasets. Moreover, several studies related to the additional damping arising from the neglect of train–bridge interaction (TBI) in the dynamic analysis have been carried out recently [18–20], but the most recent version of EN 1991–2 [12] ended up removing this criterion.

To address these gaps, the European Union Agency for Railways (ERA), together with Europe's Rail Joint Undertaking (EU-Rail) and European Committee for Standardization (CEN), issued a Technical Note [21] identifying open points in the dynamic assessment of railway bridges. Building upon this document, the InBridge4EU project [22] was launched to, among other objectives, revise the damping provisions of EN 1991–2 [12]. The present paper builds directly upon the InBridge4EU research and introduces key enhancements over previous studies:

- A substantially larger database, including over 1150 acceleration records from nearly 90 bridges in five European countries (France, Germany, Portugal, Spain, and Sweden), representing an increase of more than 65% compared with [9]. This dataset, collected through collaboration with infrastructure managers (SNCF, DB InfraGO, Infraestruturas de Portugal, ADIF, and Trafikverket), enhances statistical robustness and representativeness.
- Application of two complementary identification algorithms, the Multi-Criteria Optimisation (MCO) and Covariance-Driven Stochastic Subspace Identification (SSI-COV), benchmarked against synthetic, numerical, and field data to enhance the reliability of damping estimates.
- Integration of forced-excitation tests performed in Sweden, which provide valuable insight into amplitude-dependent and near-resonant behaviour, rarely available in previous datasets.
- For the first time since the ERRI D214 study performed almost 30 years ago in the 1990s, a re-evaluation of the normative bridge damping is being made, including a proposal for revised damping curves corresponding to a new bridge classification scheme.

Together, these advances constitute the main contributions of this work, offering a data-driven basis for updating Eurocode guidance on railway bridge damping. The paper is structured as follows: Section 1 introduces the topic and main contributions, Section 2 describes the bridge database, Section 3 details the MCO and SSI-COV formulations, Section 4 outlines benchmark validations, Section 5 presents results and data processing, Section 6 provides normative recommendations and Section 7 summarises the conclusions.

2. Bridge and measurements database

In Part 2 of the ERRI D214/RP3 [9] report, the available data for each bridge type was limited. In contrast, the present study includes a significantly larger number of bridges, as shown in Table 1. Furthermore, ERRI D214/RP3 [9] does not specify the exact number of measurements per bridge. However, in this study, the total number of measurements, and consequently, the estimated damping ratios, reaches approximately 1150, from 89 bridges, as detailed in Appendix A (supplementary material), representing a substantial volume of processed data.

Most of the measurements collected and stored in the database came from tests under railway traffic carried out by the partners from the InBridge4EU [22] project consortium. This type of tests is conducted to measure the dynamic response of the bridge in terms of accelerations caused by the passing trains. The accelerations of the bridge are recorded using accelerometers attached to the bridge deck and connected to an acquisition system that gathers all the data in a computer.

Table 1
Comparison between the bridge data used in the D214 report and in this work (InBridge4EU project).

Database	ERRI D214/RP3	Inbridge4EU	Difference (%)
Bridge type			
Steel	24	20	-17%
Composite	6	18	+ 200%
Prestressed concrete	9	13	+ 122%
Reinforced concrete		7	
Filler beam	14	24	+ 71%
Portal Frame	0	7	-
Total	53	89	+ 68%

To enhance the dataset, some forced-excitation tests in Sweden were also processed in this work. A 50 kN MTS hydraulic actuator (see Fig. 1) applied constant-amplitude harmonic loads to the bridges. Input force was measured by a load cell, and bridge responses were recorded with uniaxial MEMS accelerometers at 1200 Hz. Forced loads of 1–20 kN were applied across a frequency sweep to study amplitude-dependent nonlinearities, inducing resonance when the excitation matched the natural frequencies. Details of the instrumentation can be found in [7].

3. Damping estimation methods

3.1. Initial considerations

Damping was estimated from the free decay response of railway traffic tests using two algorithms: Multi-Criteria Optimisation (MCO) and covariance-driven Stochastic Subspace Identification (SSI-COV). This dual-method approach was adopted to enhance robustness, as damping estimation in railway bridges can be sensitive to algorithm-specific limitations, and the use of two complementary techniques helps ensure consistent and reliable results. For the Swedish forced-excitation tests, where no free decays were available, damping was computed via least-squares fitting of the frequency response function using MATLAB® [23] built-in function *"modalfit"*. Sections 3.2–3.4 briefly describes each method, and Section 3.5 outlines the procedure to define the free decay period. All natural frequencies had been previously estimated by the infrastructure managers and researchers who carried out the measurements, which allowed verification of the frequencies obtained in this work using the methods mentioned above. After confirming that the identified modes matched those from the measurement campaigns, these frequencies could be relied upon, along with the corresponding computed damping values.

3.2. Multi-Criteria Optimisation (MCO)

The MCO method reconstructs a multi-degree-of-freedom function matching the measured free-response signal in time and frequency domain. It uses MATLAB® [23] multi-objective optimisation toolbox *GODLIKE* [24], combining global and local optimisation strategies. This approach allows simultaneous multi-mode fitting without heavy filtering, improving separation of close modes. Damping estimation assumes that the measured free-response acceleration can be expressed as a sum of exponentially decaying sines given by Eq. (1), with a linear viscous damping model and constant amplitude and frequency parameters.

$$s(t) = \sum_{i=1}^{Ndof} A_i \cdot \exp(-\omega_i \cdot \xi_i \cdot t) \cdot \sin\left(\omega_i \cdot \sqrt{1-\xi_i^2} \cdot t + \phi_i\right) \quad (1)$$

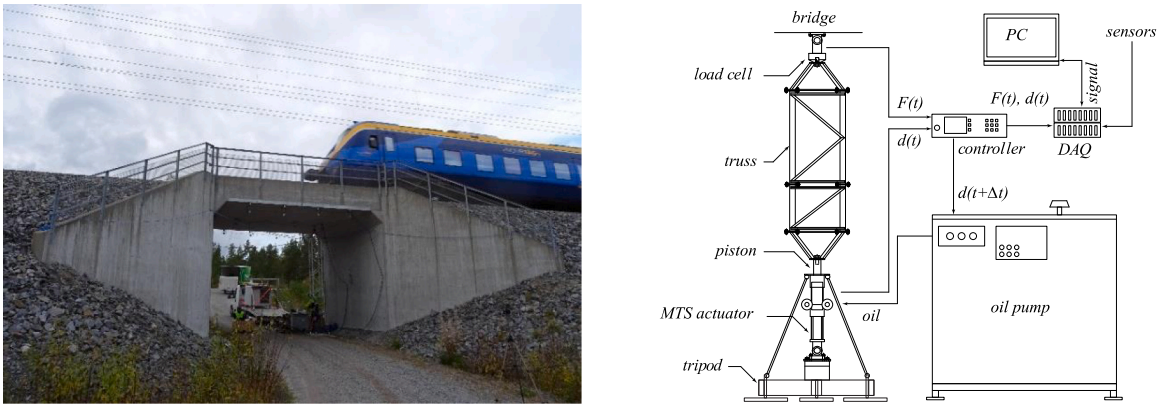

Fig. 1. Load-controlled hydraulic actuator used by KTH in the tests under forced excitation: a) installation in the Degermyran portal frame bridge tests and b) schematic.

where N_{dof} is the number of considered modes, t is time, and A_i, ω_i, ξ_i and ϕ_i are the amplitude, the angular frequency, the damping ratio and the phase of mode i, respectively. Additional variables related to the definition of the starting time of the decay and its duration do not appear in Eq. (1), but are referred to as t_0 and t_{end} later in this report. Fig. 2 exemplifies the MCO damping estimation for the Spanish bridge Tirteafuera, showing the superimposed measured and fitted signals in time and frequency domains. Details about the mathematical formulation may be consulted in [24].

3.3. Covariance Driven Stochastic Subspace Identification (SSI-COV)

The SSI-COV method, originally introduced by Peeters *et al.* [25] and widely used in civil engineering applications related to structural health monitoring [26], was adopted in this work to estimate damping from the bridge's free decay response following train passage. This time-domain method identifies a discrete state-space model from the recorded response, enabling the characterisation of the structure's dominant modes. Although initially developed for stochastic identification, SSI-COV can also be applied to extract modal parameters from free decay responses, such as those observed after a train has crossed the bridge. The observed free decays can be directly used as input to the SSI-COV method, replacing the correlation functions typically calculated from ambient responses. The contribution of specific modes to the damping values can be determined using the procedure detailed in [27] and [28].

For this work, a user-friendly Python® SSI-COV application was developed to estimate damping ratios from free decay responses. The estimation steps are illustrated in in Fig. 3 for the DB InfraGO EÜ über Stöckener Straße bridge and can be summarized as:

1) Upload the raw time series from railway tests, including sampling frequency (see Fig. 3a).
2) Filter the signal and isolate the free decay segment (see Fig. 3b) using the procedure from Section 5.4. The decay start is defined as in Section 3.5 and manually verified.
3) Execute SSI-COV on the free decay part (see Fig. 3c) to compute damping ratio ξ, mode frequency f, and vibration amplitude A with its contribution to total response. Default parameters for model order and mode clustering were used, as damping is largely insensitive to them. Spurious modes with low contribution can be disregarded (e.g., Mode 2 at 3.3%).

3.4. Least squares ratio function estimation incorporated in MATLAB's "modalfit" function

The forced excitation tests (see Fig. 1) applied constant-amplitude sinusoidal loads across frequency sweeps to induce resonance when matching natural modes. The complex-valued Frequency Response Function (FRF) $\mathbf{H}(\omega)$, given in m/s^2/kN, has been calculated according to Eq. (2) based on the input force $\mathbf{F}(\omega)$ and output acceleration $\mathbf{A}(\omega)$ in the frequency ω domain. As these test records lack free decay periods, damping was estimated using the method described by Albright *et al.* [29], which computes critical damping ratios via the least squares ratio built-in MATLAB® [23] function *"modalfit"* [30].

$$\mathbf{H}(\omega) = \mathbf{A}(\omega)/\mathbf{F}(\omega) \tag{2}$$

Fig. 4 provides an example of results for 5, 10, and 20 kN tests on the Sidensjövägen bridge (see Appendix A), where damping was evaluated from an accelerometer located at midspan [31]. The *"modalfit"* function provided good agreement between fitted and experimental FRFs, allowing several modes to be identified depending on the test and

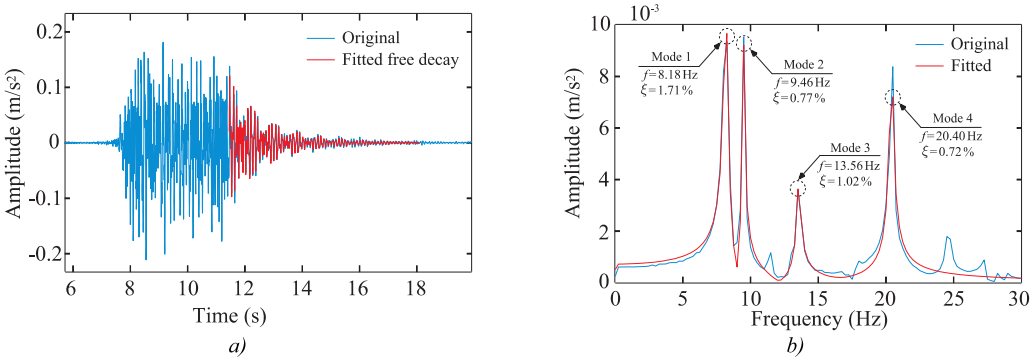

Fig. 2. Signal fitting through MCO: a) time and b) frequency domains (example with the ADIF Tirteafuera bridge).

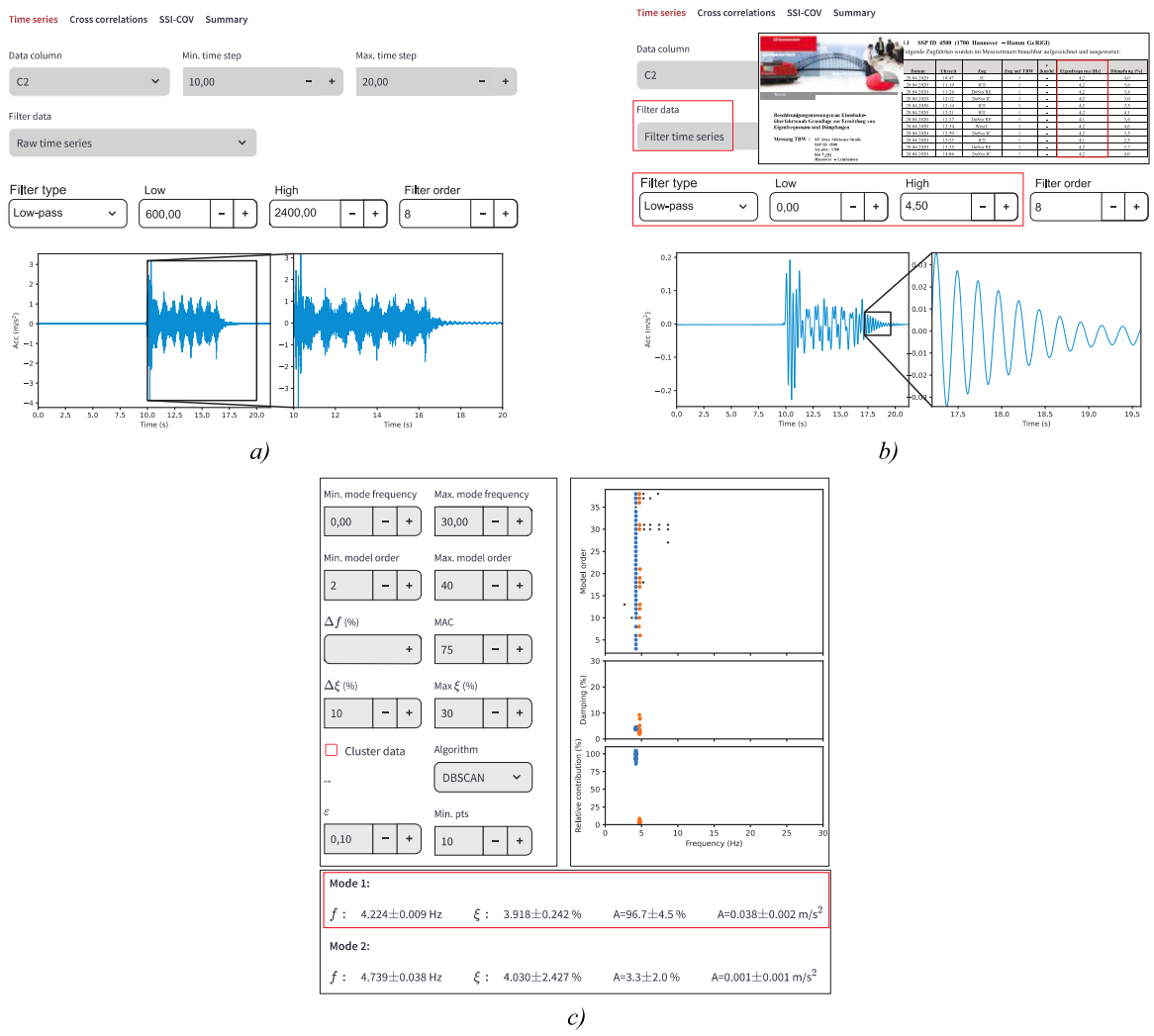

Fig. 3. SSI-COV tool developed in this work: a) step 1, b) step 2 and c) Step 3.

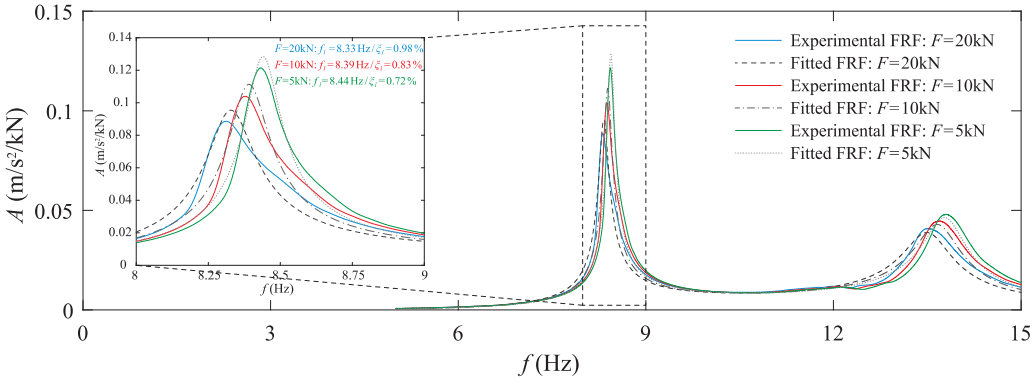

Fig. 4. FRF computed from the output response measured at the midspan and corresponding fit through the MATLAB® "modalfit" function to estimate frequency and damping on the detected modes.

frequency sweep.

3.5. Analysis of the free decay period

An automated procedure to define the initial time t_0 of the free response for damping estimation is presented in Section 3.5.1 and validated using the Portuguese dataset, which includes optical sensors detecting train entry and exit. Rules for selecting the signal end time t_{end} are described in Section 3.5.2

3.5.1. Estimation of the initial free-decay instant

Two methods, the statistical sigma and the displacement peak, were developed, both closely matching the optically detected departure time. Instrumentation setups with accelerometers and optical sensors are detailed in [10]. Optical sensors were placed at the track in both extremities of the six Portuguese bridges (nos. 1–6), while accelerometers

were located at mid-span.

3.5.1.1. Statistical sigma method. The statistical sigma method estimates the train departure time by detecting the last acceleration value exceeding a sigma threshold. The procedure, illustrated in Fig. 5a, includes:

1) Detecting the train passage using the 1 s rolling-RMS or moving standard deviation $L_{eq,1s}$, with boundaries defined where $\max\{L_{eq,1s}\} - 40$dB is reached (signal st_{train} in Fig. 5a).
2) Computing the standard deviation σ of the 600 Hz low-pass filtered acceleration to keep a broader statistical distribution of the acceleration values (signal st_{acc} in Fig. 5a).
3) The start of the free-response t_0 (train's departure time) is the time of last exceedance of σ.

3.5.1.2. Displacement peak method. The displacement peak method estimates train departure time from the last significant displacement peak, which coincides with optical sensor detection. Since displacement measurements are sensitive to low frequencies, these peaks are presumed to correspond to the passage of each bogie. The process, illustrated in Fig. 5b, involves the following steps:

1) Double acceleration integration to get displacement, applying a 1 Hz high-pass filter to avoid drifting.
2) An automated process, involving normalization, peak detection, weighting, and thresholding, identifies the last valid peak and, consequently, the initial time of the free-response t_0

3.5.1.3. Validation with data from the optical sensors. Both methods were validated using optical sensor data from six Portuguese bridges (Appendix A includes four of these cases, for which damping could be estimated), enabling experimental identification of train entry times (see [10] for instrumentation details). Fig. 6a compares t_0 estimates with reference values, showing median differences, and Fig. 6b shows the same data coloured by train speed. Despite some spurious speed values, the following observations were made: *i)* most absolute errors are below 100 ms; *ii)* sigma method performed best except on bridge 4, with median errors 0.5–37.6 ms; *iii)* Bridge 4 performs worst, likely due to low train speeds (20–60 km/h). Based on these results, the sigma method has been adopted in this work.

3.5.2. Selection of the free-decay duration

Two approaches have been applied to set rules for the selection of the instant t_{end} where the free-decay finishes:

- Damping calculated with SSI-COV: a fixed number of 10 periods of the first fundamental bending frequency was considered in this case (e.g., a 5 Hz mode implies a duration of 2 s).
- Damping calculated with MCO: t_{end} is the point where RMS value dropped 40 dB as compared to t_0, which corresponds to a ratio of 100 on amplitude between starting and ending times.

Depending on passages, the t_0 and t_{end} value could be adjusted manually to focus damping estimation on certain parts of the signal or avoid disruptive parts.

4. Benchmark tests

4.1. Initial considerations

This section compares the performance of the two damping estimation methods, MCO and SSI-COV, using free decay periods from railway traffic tests. The comparison includes:

- Artificially generated signals with linear damping (Section 4.2).
- Signals from TBI analyses using FEM models (Section 4.3);
- Real bridge test data (Section 4.4).

4.2. Linear damping test cases

The first validation used artificially generated time series with known damping to test both MCO and SSI-COV under controlled conditions. By comparing estimated and predefined values, the methods' accuracy and reliability were assessed, enabling direct comparison between the two algorithms. Thus, artificial signals $s(t)$, representing a free-decay vibration with steady-state and damped components, may be defined to test the damping estimation algorithms through the same Eq. (1) presented above. For a more representative benchmark, gaussian noise, dependent on the mean μ_i, standard deviation σ_i and amplitude ratio R_i of the signal relative to degree of freedom i, has been added to the signals.

For this validation, 10 test signals were generated with 1–3 degrees of freedom N_{dof}, each having distinct frequencies and damping, allowing to cover a wide range of scenarios. The start of the free decay is $t_0 = 8$ s and the end $t_{end} = 20$ s for all the scenarios. Fig. 7 shows the damping estimations obtained using the MCO and SSI-COV methods for one of the test signals with $N_{dof} = 2$. A perfect correspondence can be observed between the imposed damping ($\xi_1 = 1\%$ and $\xi_2 = 0.5\%$) and frequencies ($f_1 = 5$ Hz and $f_2 = 6.5$ Hz) and those estimated by both methods, demonstrating their accuracy in this context. The same full level of agreement was observed for all other nine signals, that are not shown

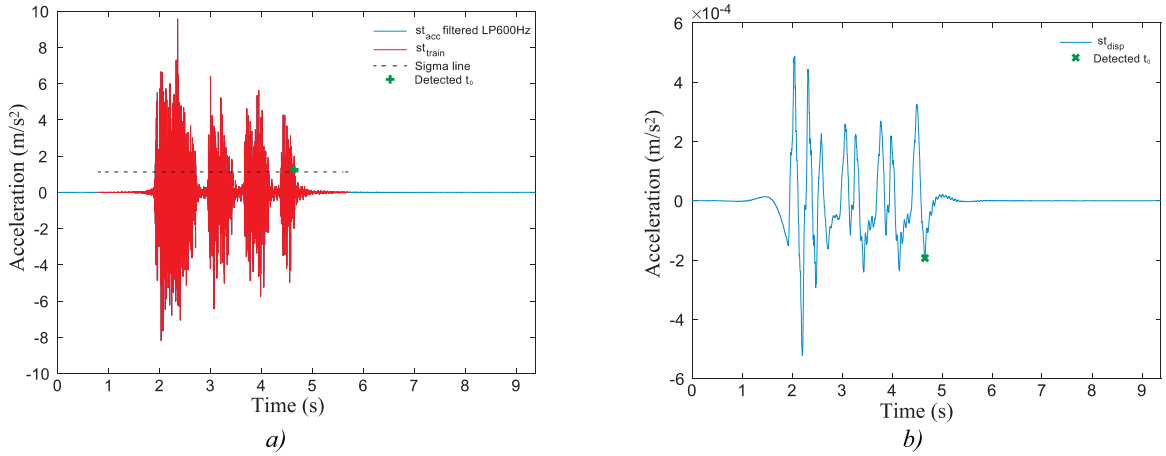

Fig. 5. Detection of t_0 with the a) sigma method and b) displacement peak method.

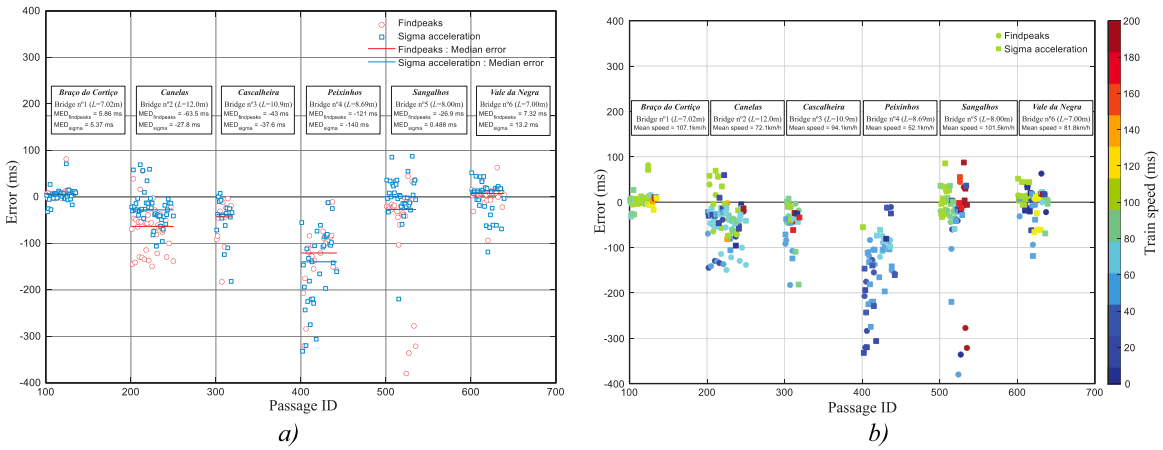

Fig. 6. Error between the two t_0 detection methods against optical sensor reference: a) with median estimators, b) with train speed estimation.

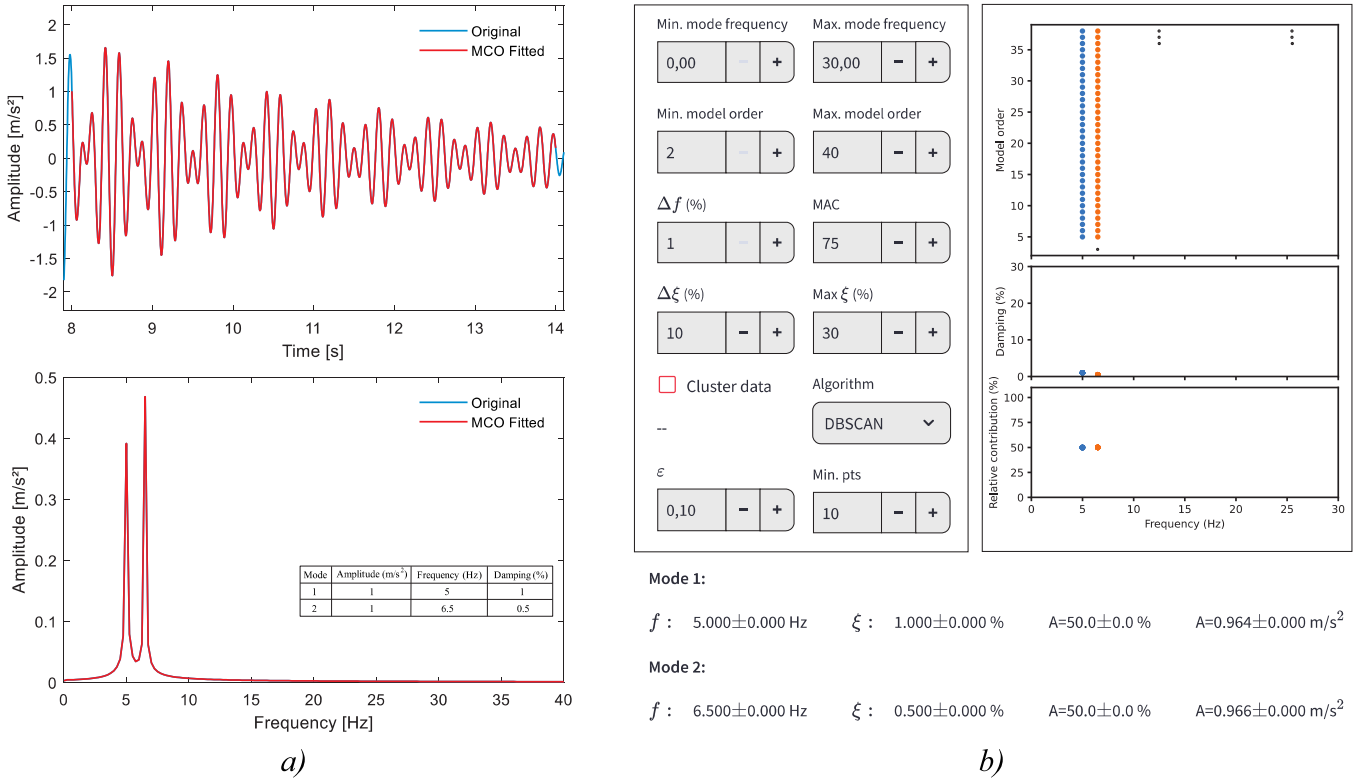

Fig. 7. Validation test No. 5: a) free decay period of the artificially generated time series and correspondent identification with MCO and b) with SSI-COV.

due to space limitations.

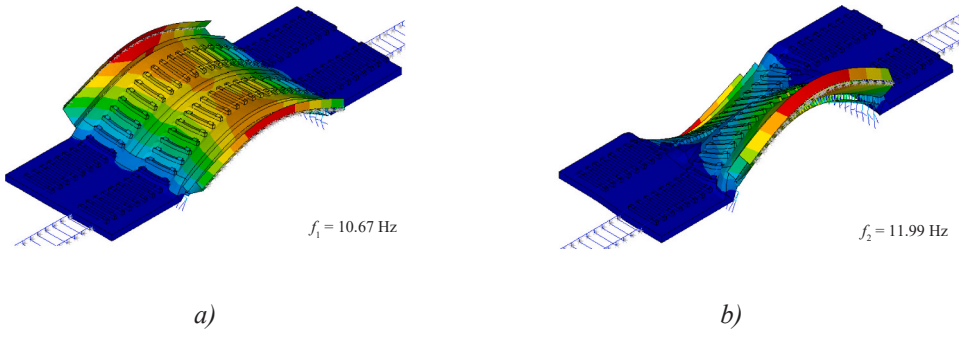

Fig. 8. Numerical mode shapes of the Cascalheira bridge: a) bending and b) torsion.

4.3. FEM test case

A second test case consisted of simulating responses from one of the bridges from the database, the 11 m span filler-beam Cascalheira bridge in Portugal, through TBI dynamic analysis. A detailed 3D finite element model, described in detail in [32], was developed in ANSYS® (2019). Concrete components were modelled with shell elements, steel girders and rails with beam elements, and ballast and sleepers with solid elements. The model was calibrated to match experimentally identified modes and train-induced responses [32].

The numerical modal shapes of the first two modes of vibration (vertical bending and torsion) and its correspondent natural frequencies are depicted in Fig. 8.

Regarding the vehicle, a multibody model of the Alfa Pendular train was also developed in ANSYS®. The model consists of 6 cars, each one with seven rigid bodies (one carbody, two bogies and four wheelsets) connected through the primary and secondary suspensions (details of the vehicle may be consulted in [32]).

The dynamic analyses have been carried out with a TBI tool developed and validated by the authors [33]. Ten simulations were carried out, in which the Alfa Pendular train crossed the bridge at 135 and 165 km/h under four measured track irregularity profiles described in [10]. Due to the direct-integration approach, damping was considered using a Rayleigh proportional matrix. Hence, in the first eight tests (two speeds and four irregularity profiles), a target damping ratio of 2.12%, as specified in EN 1991–2 [12] for this bridge type, was adopted for the two global modes shown in Fig. 8. In the other two tests (165 km/h), different damping ratios were assigned to each mode, namely 2.2% and 2.4% for test 9, and 4.2% and 4.7% for test 10.

Fig. 9 compares the FEM reference frequencies and Rayleigh-imposed damping with the estimations from both methods. Except for test case No. 4, where MCO largely overestimated the bending mode damping, both methods showed good agreement with the target values, independently of its magnitude, confirming their reliability for damping estimation.

4.4. Real signals test cases

Although artificial noise was added to synthetic tests, real field data introduce further complexity, such as nonlinear effects, transients, and irregular decays, that hinder damping estimation. Controlled cases are therefore necessary but insufficient for full validation. To assess reliability, 33 train passages from various countries and conditions were analysed using SSI-COV and MCO methods. Detailed results are presented only for the 14 m span *"U"*-shaped composite Savigny-le-Temple (830000_036 +790) bridge in France, while the remaining results are summarized at the end of this section. Five passages were considered, with decay start and end times kept undisclosed between users to ensure unbiased benchmarking. Fig. 10 shows passage no. 62, while Table 2 summarises the results. SSI-COV used 10 cycles for damping estimation, while MCO selected t_0 and t_{end} as per Section 3.5. Despite differences in the signal segment length, damping ratios agreed within 0.5%pt, confirming both methods' reliability.

Fig. 11 summarizes the results from all 33 benchmark tests for first-mode frequency and corresponding damping. Frequency estimates generally agree within 0.2 Hz, except for the Sermaize benchmark, whose strong non-linear free decay likely explains the discrepancy. Regarding damping, Fig. 11b shows overall good agreement between the two methods for the fundamental mode, though some cases deviate notably (e.g., Guadiana 1, which yielded a non-physical negative value). Still, most differences remain within 0.5%pt. The cases where large discrepancies have appeared are generally due to the following reasons:

- Non-linear behaviour of the free-decay (e.g. Sermaize example).
- Complex signals with very short or very long duration, broad frequency content, or high noise (e.g., Braço do Cortiço 3, Sarstedt 3, Vinzelberg 1, Kerpen 17).
- First mode not predominant, making identification harder (e.g., Guadiana 4, Malay 31).

5. Results and data processing

5.1. Initial considerations

This section presents the damping ratios estimated for all analysed bridges using the algorithms introduced and benchmarked in Sections 3 and 4. About 1150 train passages over 89 bridges in Portugal, Sweden, Spain, Germany, and France were examined. Damping coefficients for the fundamental vertical bending mode ξ_1 are plotted against span length L and bridge type, with full data provided in Appendix A. The analysis first examines the influence of response amplitude on damping estimates (Section 5.2), then the potential for statistical treatment (Section 5.3), and finally identifies near-resonance scenarios where damping most affects design (Section 5.4), forming the basis for the recommendations in Section 6. Fig. 12 shows ξ_1 versus span L, grouped by bridge type per EN 1991–2 [12] (portal frames are included with reinforced-concrete types due to structural similarity). Despite significant scatter, most damping ratios exceed EN 1991–2 [12] limits, with a few lower outliers discussed later.

5.2. Influence of the response amplitude in the damping values

The correlation between vibration amplitude and damping was first examined. ERRI D214/RP3 [9] reported only a slight correlation

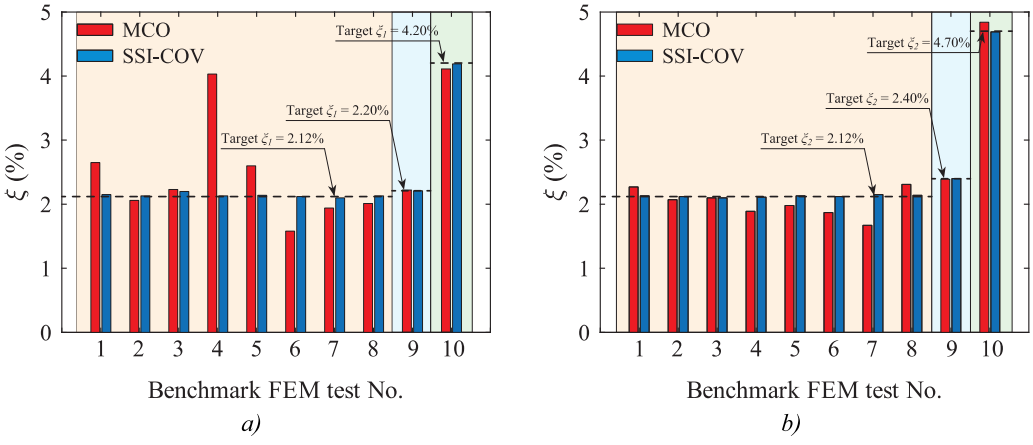

Fig. 9. FEM benchmark damping results: a) mode 1 – bending, b) mode 2 - torsion.

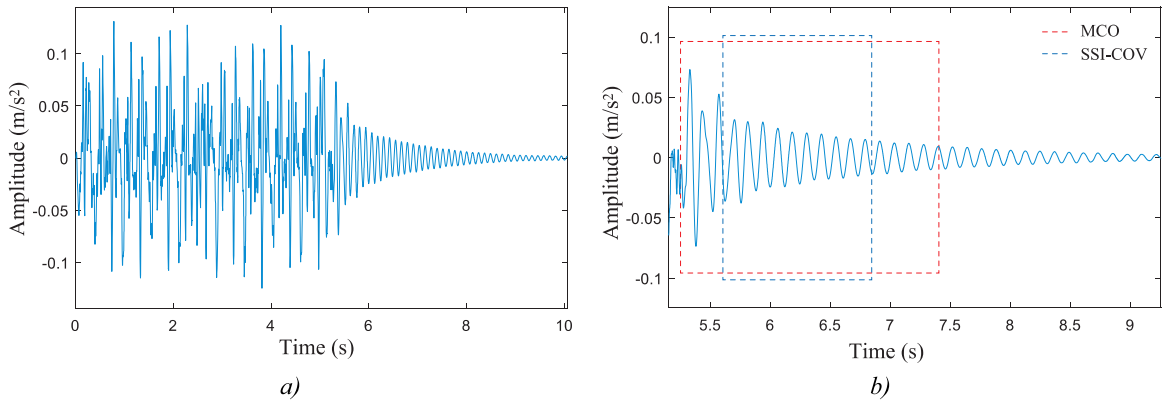

Fig. 10. Response of the Savigny bridge test case no. 62: a) whole time signal and b) zoom on free decay.

Table 2
List of Savigny test cases and SSI-COV and MCO estimates of damping and frequency.

Test case id	MCO			SSI-COV		
	f_i (Hz)	ξ_i (%)	A_i (m/s²)	f_i (Hz)	ξ_i (%)	A_i (m/s²)
830000_036 + 790 33	8.16	1.84	0.070	8.21	1.40	0.076
830000_036 + 790 60	8.21	1.36	0.023	8.25	1.17	0.025
830000_036 + 790 62	8.18	1.80	0.055	8.22	1.31	0.039
830000_036 + 790 71	8.22	1.03	0.013	8.33	1.18	0.016
830000_036 + 790 81	8.23	1.86	0.044	8.27	1.19	0.032

between free decay amplitude and estimated damping, clear in some bridges (e.g. Vieux Briollay, Valenton) but absent in others (OA 49/25 viaduct, Bip bridge). Fig. 13 shows damping coefficients for the first bending mode versus acceleration amplitude in seven bridges, displayed in two subfigures due to amplitude-scale differences (the amplitudes correspond to the filtered signals used to estimate damping, following the procedure described in Section 5.4). While some cases (e.g. Taxinge, 00100–186 +312) indicate higher damping with increasing amplitude, most do not follow this pattern. Other bridges, not shown here, confirm the lack of consistent correlation. Overall, the results suggest that assessing amplitude effects on damping is difficult, as acceleration levels were mostly below 0.3–0.4 m/s², so variations across tests were not sufficiently pronounced to differentiate the damping outputs and support firm conclusions. It is worth to refer that in the tests under forced excitation by the actuator carried out in Sweden, damping was generally higher when the applied force was larger, although the differences were not very significant.

5.3. Feasibility of performing statistical analysis of the results

Given the wide range of bridge measurements, a statistical analysis was performed using the ÖBB-Regelwerk 08.01.05 [34] procedure, which follows EN 1990-Annex D [35] specifications, to assess its validity for defining reliable lower bounds of damping. According to this statistical procedure, the 5% fractile (characteristic value) of a property, in this case the bridge damping, should assume a Normal/Log-Normal distribution and an unknown mean value. Based on these assumptions, damping ξ_d is determined as the 5% fractile for a 75% confidence level a

$$\xi_d = \eta_d \bullet (\bar{\xi} - k_n \sigma) \tag{3}$$

where $\bar{\xi}$ is the empirical mean from the tests, σ is the standard deviation, η_d a data-quality factor (1.0 for good, 0.9 for average), and k_n a factor retrieved from [34,35] for unknown standard deviations. The factor k_n decreases as the number of tests increases, approaching 1.64, which corresponds to the 95% value of a standard normal distribution. Thus, a larger number of tests ensures a more reliable statistical fractile.

Results obtained from a 2-year measurement long-term monitoring campaign in the 48 m Bryngeån composite bridge in Sweden indicated that, while the frequency values fitted a generalized extreme value distribution, damping did not follow any conventional distribution [14]. This suggests that assuming a Normal distribution for damping is not

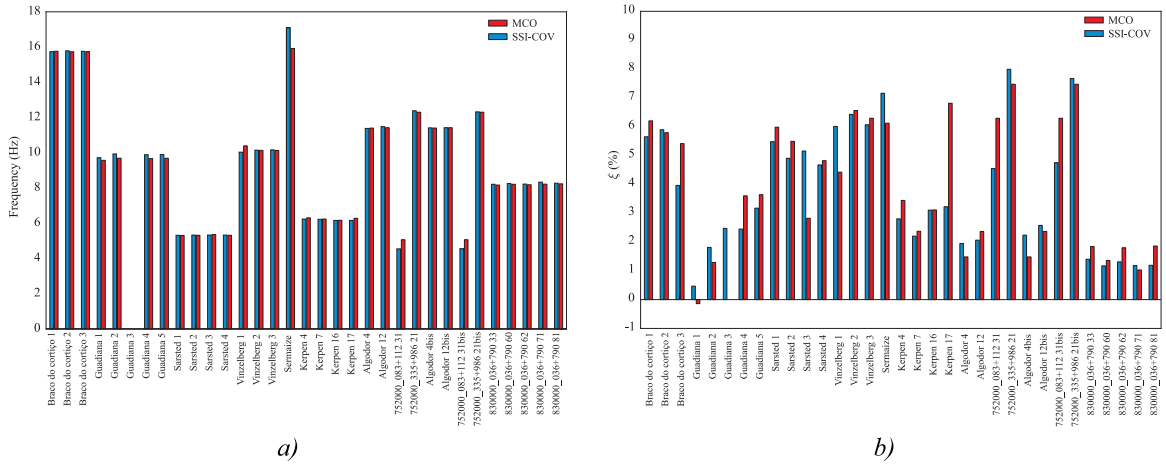

Fig. 11. Results obtained in the real case benchmark: a) estimated frequencies and b) damping relative to the first fundamental bending mode of vibration.

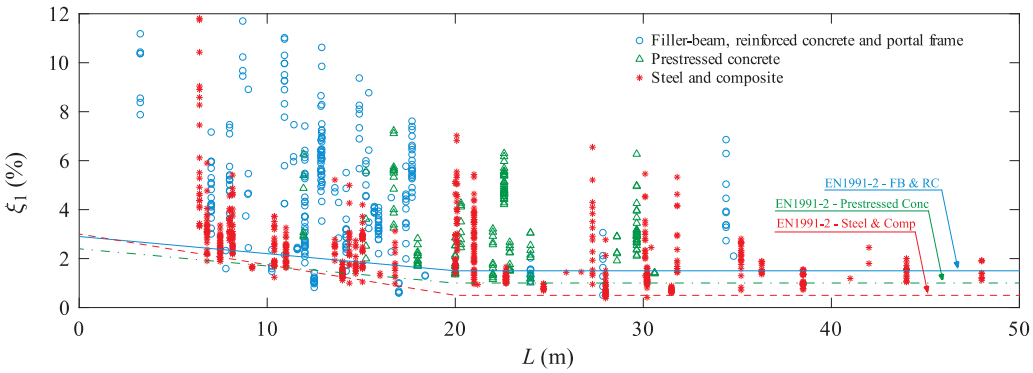

Fig. 12. Damping coefficients related to the first bending mode as function of span and EN 1991–2 [12] bridge types.

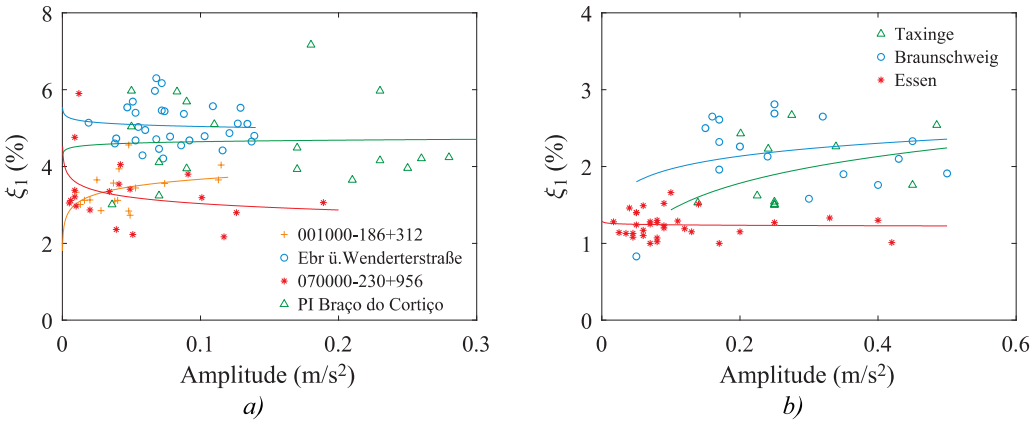

Fig. 13. Damping coefficients related to the first fundamental bending mode as function of the acceleration amplitude of isolated bridges: bridges with maximum amplitude of a) 0.3 m/s^2 and b) 0.6 m/s^2.

entirely valid, though the statistical analysis was retained for clarity.

A statistical analysis was conducted on a subset of bridges to assess the method's suitability for damping evaluation. The selected cases (see Table 3) covered various bridge types, spans, and levels of data scatter. Using Eq. (3) with n and k_n and assuming good-quality data (η_d=1.0), the 5% fractile damping ξ_d was computed. Results show that, due to high scatter and limited samples, the 5% fractile often falls below the estimated lower bound, improving only for bridges with more consistent data (e.g. Ebr ü.Wenderterstraße, Essen, Ponte de Canelas). For sparse or highly variable datasets (e.g. 590000_235 +895, Bracea), values become overly conservative or even non-physical (negative damping values).

The large damping scatter observed (see Fig. 12) is typical of railway traffic measurements and limits statistical reliability, as damping is influenced by multiple uncontrolled factors, such as material dissipation, friction, structural condition, and soil–structure interaction. Combined with small samples and non-normal distributions, this undermines the fractile-based approach in [34], often yielding excessively conservative results. Consequently, the lower bounds of measured damping values, rather than statistical fractiles, were adopted to guide the recommendations proposed here.

5.4. Evaluation of the contribution of the fundamental vertical bending mode for the bridge response

The next step was to identify near-resonant cases, where damping most affects bridge design [9]. Thus, since scenarios far from resonance can yield misleading results, a consistent procedure is required. In bridges more prone to resonance, such as simply supported, vertical resonance under repeated axle loads typically involves the global bending or torsional modes. The fundamental bending mode is the most critical, as for higher modes, matching between axle spacing and bridge frequency can cause opposing forces on upward and downward sections, partially cancelling resonance and diminishing their overall influence on

Table 3
Selected bridges for statistical analysis and respective parameters and 5% fractile value ξ_d.

Bridge name	Country	Type	Span (m)	n	k_n	Range ξ (%)	$\bar{\xi}$ (%)	σ (%)	ξ_d (%)
Nuthe Drewitz - ID23194	Germany	Filler beam and reinforced concrete	17.70	20	1.76	4.70 – 7.61	6.02	0.84	4.55
Aspan	Sweden		24.00	10	1.92	1.07 – 2.03	1.41	0.28	0.86
282.943 - Ponte de Canelas	Portugal		12.00	13	1.87	1.61 – 5.34	3.25	0.83	1.69
Södra Kungsvägen	Sweden	Portal frame	15.25	7	2.09	4.54 – 6.00	5.28	0.59	4.05
Bracea	Spain	Prestressed concrete	15.25	4	2.63	1.99 – 5.57	3.42	1.58	-0.75
Ebr ü.Wenderterstraße - ID5046	Germany		22.60	31	1.73	4.21 – 6.30	5.06	0.54	4.13
590000_235 + 895	France	Steel-concrete composite.	6.40	22	1.75	3.31 – 11.81	6.30	2.74	1.50
242000_138 + 166	France		31.50	21	1.76	0.60 – 0.89	0.71	0.08	0.57
Augsburg - ID31962	Germany	Steel	20.08	11	1.90	3.43 – 7.02	5.01	1.18	2.77
Essen - ID17028 | 17553	Germany		22.70	35	1.72	1.00 – 1.66	1.24	0.16	0.96

the bridge response. Torsional modes may also resonate, especially in double-track bridges, which sometimes may be coupled with bending (e.g. Silva *et al.* [10]), complicating damping estimation.

Since the first global modes dominate train-induced resonance, damping should be derived mainly from responses governed by the first vertical bending mode. This mode is easily captured with midspan sensors, unlike torsional modes that require larger instrumentations setups, which are not always available in the datasets. As most datasets provided only the first bending frequency, near-resonant cases were defined as those characterized by responses dominated by this mode, ensuring that only relevant damping values were used for normative purposes. It should be noted that these records do not necessarily represent a true resonance, where the axle passage frequency matches the bridge's natural frequency, but they are more representative of such conditions, as the response is mainly governed by a single mode, as typically observed under global deck resonance. This represents an improvement over the ERRI D214 work [10], which lacked a quantitative evaluation of this contribution. Considering this rationale, the following procedure is proposed to assess damping in near-resonant scenarios:

1) Estimate the frequency of the bridge's fundamental vertical bending mode f_1 using Infrastructure Managers' dynamic reports or ambient vibration tests, when available. This step will help determine the fundamental mode frequency in advance, making it easier to identify it in the subsequent analysis.
2) Apply a low-pass filter to the time series with a cutoff frequency f_{cut} given by the following equation proposed by DB InfraGO in its dynamic measurement reports:

$$f_{cut} = \max\{30\ \text{Hz},\ 9f_1\} \tag{4}$$

   where the 30 Hz value is based on the procedure from [36] for evaluating deck acceleration, while the $9f_1$ corresponds to a procedure from DB InfraGO to assess the contribution of higher-frequency modes.
3) Extract the free decay segment.
4) Apply MCO or SSI-COV to this segment to estimate the modal properties of the fundamental bending mode, together with its percentage contribution to the overall response.
5) Retain only cases where the amplitude of the fundamental mode dominates the overall response.

Fig. 14a depicts an example of a free decay response of a measurement on the German bridge Ebr ü.Wenderterstraße clearly dominated by the first vertical bending mode, which contributes with 82% to the total acceleration amplitude. In contrast, Fig. 14b shows a scenario from the French bridge 001000_459 + 633, where the fundamental mode contributes only 17% to the overall response. In the present work, only the damping ratios derived from scenarios equivalent to those presented in Fig. 14a were considered for normative recommendations

Following the procedure described above, damping ratios are shown for each bridge category, separating near-resonant from non-resonant cases (grey), excluded for normative recommendations. As a result, of the 1150 measurements, about 200 were removed. The results show higher lower bounds for most bridge types, though particularly low values still need careful consideration to avoid skewing the results. The final validated damping ratios form the basis of the normative proposals presented later in Section 6.

5.4.1. *Filler beam and reinforced concrete bridges*

For the *"filler beam and reinforced concrete"* category, some valid damping estimates fall below the EN 1991–2 [12] curve (see Fig. 15), particularly for Swedish bridges, even when considering forced vibration tests. These structures, featuring 1.5–2.0 m over-sails (deck overhang beyond the abutment support), are common in Sweden, but atypical in the wider European context. Moreover, most Swedish bridges are equipped with pot bearings, which may dissipate less energy at the supports than roller or elastomeric bearings, suggesting that national provisions could be considered to account for their influence and avoid overly conservative general recommendations. However, even excluding them, a few bridges from France and Portugal still show values below or close to the current damping normative curve. Given the proven adequacy of the existing damping ratios in bridge design practice over the past, there is no engineering basis to justify lowering the current normative curve.

5.4.2. *Portal frame bridges*

The results presented in Fig. 16 demonstrate a clear overall trend for the *"portal frame"* bridge category, which is not currently addressed in EN 1991–2 [12], with damping ratios consistently well above the normative curve for the closest structurally comparable family, the reinforced concrete bridges, mainly due to radiation damping from backfill soil. The only exceptions occur in the longer-span Gesällgatan North and South bridges ($L \approx 30.6$ m, with damping ratios close to 1.5%), which are prestressed and may also be classified as such (to be addressed later), since their low frequencies do not give rise to significant soil–structure interaction [37] and their damping approaches the normative limits. Nevertheless, portal frames are particularly common in Europe for shorter spans, typically below 20 m, so these deviations do not compromise the proposed normative recommendations for this bridge category.

Supporting this high damping trend, the CEN/TC250/SC1 report [38] summarises measurements on Austrian portal frames with spans up to 20 m conducted by ÖBB-Infra, showing damping between 5.5% and

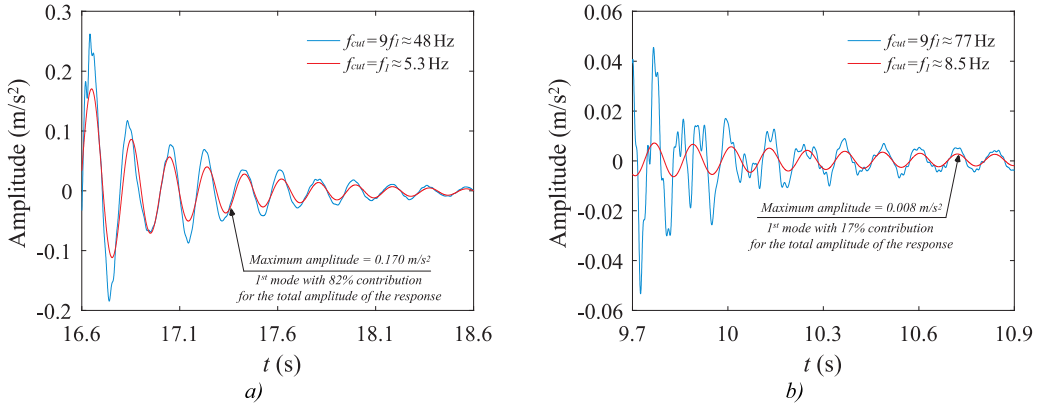

Fig. 14. Free decay response where the fundamental first vertical bending mode is a) dominant (bridge Ebr ü. Wenderterstraße in Germany); and b) not dominant (bridge 001000_459 +633 in France).

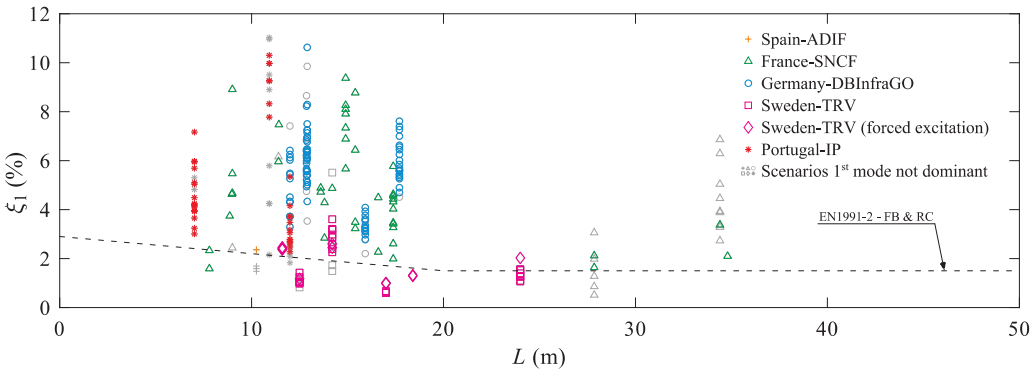

Fig. 15. Damping ratios that are not majorly controlled by the fundamental vertical bending mode for the filler beam and reinforced concrete bridge category.

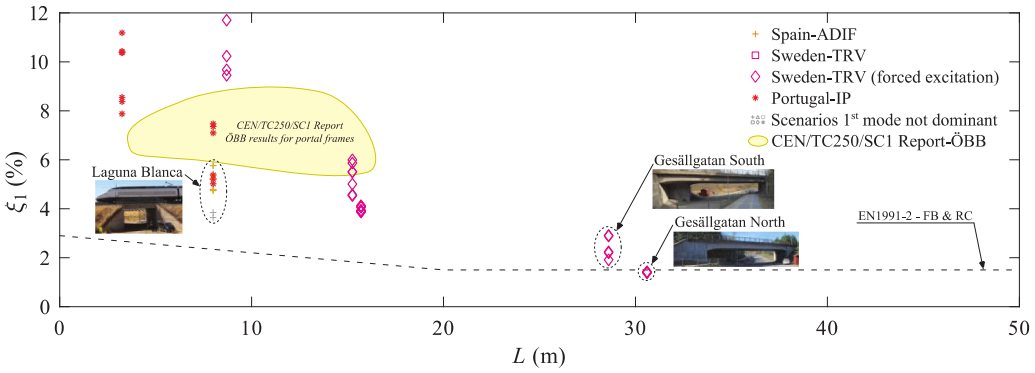

Fig. 16. Damping ratios that are not majorly controlled by the fundamental vertical bending mode for the portal frame bridge category.

8.8% for 4–16 m spans, consistent with the present study (depicted in Fig. 16 for reference). This agreement, although based on estimations derived from different methods and outside the scope of this work, further reinforces the case for including portal frames in the normative damping definitions for railway bridges, as will be discussed later in Section 6.

5.4.3. *Prestressed concrete bridges*

Most damping ratios from non-resonant scenarios in prestressed concrete bridges are low, with some close to the current normative curve (see Fig. 17). When these are excluded, the lower bounds are generally higher than current values, suggesting that a revision towards higher damping could be justified. The lowest ratios, $\xi_1 = 1.34\%$ and 1.38%, correspond to the Swedish bridges Enköpingsvägen ($L = 20$ m) and Gesällgatan North ($L = 30.6$ m), whose over-sail configurations and pot-bearing supports may account for the reduced energy dissipation, rendering them atypical in the European context.

Enköpingsvägen shows an unusual trend, with higher damping under railway traffic ($\xi_1 = 1.79$–2.52%) than under forced excitation ($\xi_1 = 1.34$–1.51%), despite the higher acceleration amplitudes in the latter. A similar pattern appears in the Swedish Taxinge bridge ($L = 22.9$ m), but with comparable amplitude levels in both the test types ($A_1 = 0.139 \sim 0.485\, m/s^2$ under railway traffic and $A_1 = 0.250 \sim 0.450\, m/s^2$ under forced excitation, see Appendix A), making its results more representative. For Gesällgatan North, no valid railway data were available, and its portal-frame similarity limits comparison with typical prestressed configurations. Its low damping (≈1.5%) matches the normative value for reinforced and filler-beam bridges, giving little reason to maintain separate curves. This is consistent with the unclear distinction proposed in ERRI D214/RP3 [9], which lacks evidence supporting systematically lower damping in prestressed structures. A plausible explanation is that prestressed bridges are less prone to cracking, which could lead to lower damping, but no evidence is shown in the report.

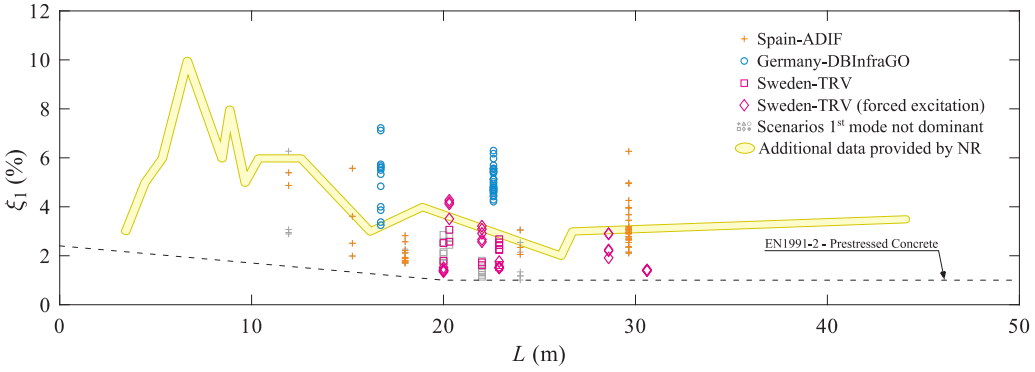

Fig. 17. Damping ratios that are not majorly controlled by the fundamental vertical bending mode for the prestressed concrete bridge category.

Finally, complementary data from Network Rail bridges (3.5–45 m spans) indicate $\xi_1 = 2$–10%, though the presence of concrete joints connecting independent prestressed elements may increase damping. Despite structural and methodological differences, these data confirm the general trend and further support the proposed enhancement of current normative specifications, as discussed in Section 6.

5.4.4. Steel-concrete composite bridges

This study examines the feasibility of splitting the current *"steel-concrete composite"* family into two bridge types, therefore, Fig. 18 shows damping ratios for the proposed *"steel-concrete composite"* type by span and country. It can be observed that non-resonant scenarios still account for some of the lower damping values (grey markers), but even when these are disregarded, for spans under 15 m the lower bound continues to align with the normative curve. The situation differs for most longer-span bridges above 20 m, which generally exhibit a damping lower bound above the current steel bridge value of 0.5%. Exceptions are two French bridges, 810000_097 + 770 (L = 24.7 m) and 242000_138 + 166 (L = 31.5 m), which, although still above the normative limit, show low damping values with little scatter: ξ_1 = 0.73–0.99% and ξ_1 = 0.60–0.89%, respectively. This behaviour is likely related to their structural design, consisting of single-track bridges with the lower flanges of the lateral inclined girders connected by spaced transversal steel girders encased in concrete (see typical cross-section in Fig. 18 and details in Appendix A for each bridge) characterized by low mass (~11 t/m), similar to the "*U*"-shaped bridges for spans up to 20 m with a steel sheet at the bottom commonly used in France (as exemplified by the 070000_219 +422 bridge with L = 9.2 m presented in Appendix A). Hence, although above 0.5%, these cases will be handled individually within the normative damping proposal for the steel-concrete composite bridge category discussed in Section 6.

For a broader perspective, the ERRI D214/RP3 [9] results for composite bridges were revisited and also plotted in Fig. 18 (spans larger than 50 m are plotted in L = 50 m for fitting purposes). Although estimated using different algorithms, making direct comparison less reliable, the data still provide valuable insights for reference. Hence, this work revisits the results from [9] for this bridge category, highlighting the following: *i)* all damping ratios were estimated using the basic LD method, which has limitations when the first mode is not well isolated, potentially affecting accuracy, and *ii)* the number of cycles used varied widely (5–88), reducing the reliability of direct comparisons.

Assuming the previously mentioned limitations are acknowledged, the following main conclusions can be drawn from the ERRI D214/RP3 [9] data:

- The Massy–Lyon (Pompadour OA49/25, L = 46.00 m) and Bebra–Göttingen (PK 238.220, L = 13.00 m) bridges show considerably high damping, thus not influencing the lower bound.
- The Le Mans–Angers (Vieux Briollay PK 293.020, L = 38.00 m) bridge presents notably low damping (ξ_1 = 0.57%), with results considered reliable despite the less accurate LD method.
- The Paris–Lille (Saint Denis PK 6.382, L = 59.80 m) bridge was analysed by two entities, LREP and SNCF-VR10, with lower bound estimates of 0.41–1.60%, respectively. According to the report, the former analysis relied on an excessive number of cycles (88) and a less accurate approach, namely a graphical determination of the LD using log paper, whereas the latter stated that the estimated value was correct, further supporting the conclusion that the results obtained by the latter are more credible.
- The Paris–Saint Lazare (Maison Lafitte, L = 66.00 m) bridge results, also obtained by LREP, were questioned by the ERRI D214 committee due to inconsistencies in the reported frequency (the committee noted that a 66 m span bridge could not plausibly exhibit a first bending frequency of 14.3 Hz) as well as the use of an excessive number of cycles (88) and manual application of the LD method with log paper. Consequently, the estimated damping ratio of ξ_1 = 0.70% is considered unreliable for normative purposes.

In summary, among the five composite bridges analysed by the ERRI D214 committee, three exhibited relatively high damping above 1%, one showed unreliable low values due to methodological issues (Maison Lafitte), and one credible low damping values in the range of 0.57–0.90% (Vieux Briollay). Despite methodological differences preventing direct comparison, all but the latter align with the overall lower bound for composite bridges shown in Fig. 18, which may be slightly above the current 0.5% for longer spans.

5.4.5. Steel bridges

The overall lower bound of damping for steel bridges (see Fig. 19), after excluding non-resonant cases, generally matches the current EN 1991–2 [12] normative curve. As with the "*filler beam and reinforced concrete*" category, the results obtained for the steel bridges show no significant deviations from this trend. Although a few cases lie slightly below the curve, they are not considered critical, given the proven performance of bridge designs over the past three decades. Hence, the available evidence provides no engineering rationale for revising the current normative damping curve for steel bridges.

6. Normative recommendation on railway bridge damping

6.1. Initial considerations

While Section 5.1 presented the damping ratios for 88 bridges based on over 1150 measurements, Section 5.4 focused on processing and critically analysing these results to exclude non-resonant scenarios and interpret deviations from the general trend. This analysis provides the basis for the normative proposals outlined in Sections 6.2–6.6, aiming to promote more economical bridge design without compromising

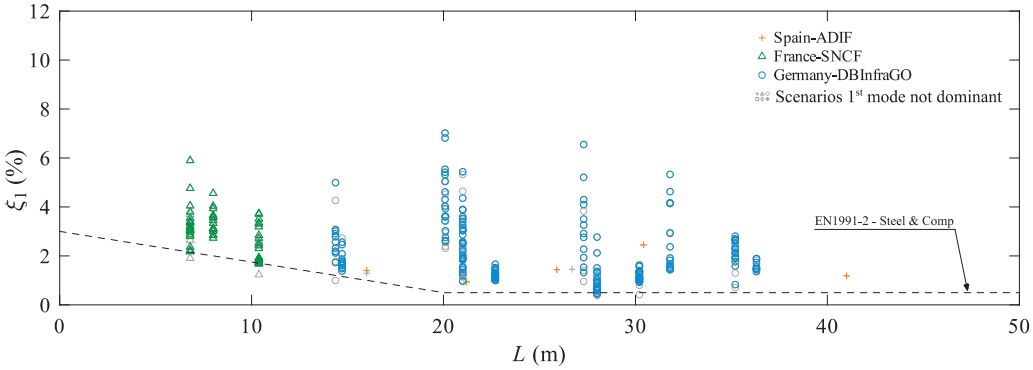

Fig. 18. Damping ratios that are not majorly controlled by the fundamental vertical bending mode for the steel-concrete composite bridge category.

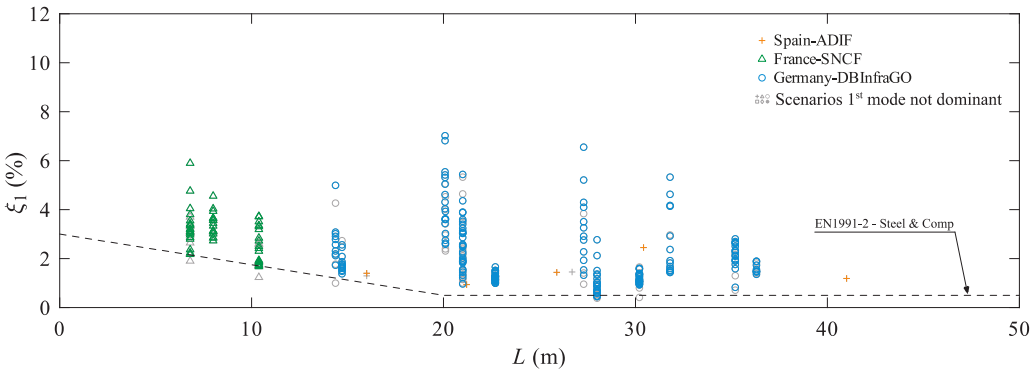

Fig. 19. Damping ratios that are not majorly controlled by the fundamental vertical bending mode for the steel bridge category.

structural integrity or train running safety.

6.2. Normative recommendations for the "filler beam and reinforced concrete" bridge type

Even after excluding non–near-resonant scenarios, several valid estimates for *"filler beam and reinforced concrete"* bridges still align with or fall below the current normative curve, particularly for Swedish bridges, but also some from Portugal and France. Given the overall lower bound, slightly below that obtained in ERRI D214/RP3 [9] (see Fig. 15), there is no engineering rationale to revise the current curve. However, results suggest that damping values from forced excitation tests are generally higher and more consistent than those from railway traffic, indicating that future controlled excitation tests on typical bridge types could provide more accurate damping estimates. Results obtained by Reiterer et al. [8] corroborate this assumption, showing that such tests generally yield higher damping values and reduced measurement scatter.

6.3. Normative recommendations for the "portal frame" bridge type

Although portal frame bridges are not covered by EN 1991–2 [12], the results presented in Fig. 16 show that spans below 20 m exhibit noticeably higher damping than comparable *"reinforced concrete"* bridges. Therefore, a new normative damping curve is proposed based on these findings, encompassing the observed lower bounds and aligning with the values from the two long-span portal frames / prestressed concrete bridges (Gesällgatan North and South).

Fig. 20 compares the EN 1991–2 [12] damping curve for *"filler beam and reinforced concrete"* bridges with the lower-bound estimates and the new proposal developed in this study. The proposed *"portal frame"* curve adequately covers the observed lower bounds, including those reported by ÖBB in [38], while significantly increasing the current normative values. For larger spans ($L > 20$ m), the limited available data, only from Gesällgatan North and South, suggests damping values consistent with the existing curve. To ensure a smooth transition, an intermediate segment was introduced for 15 m $\leq L \leq$ 20 m. The resulting piecewise function plotted in Fig. 20 defining damping as a function of span L is given by:

$$\begin{cases} \xi = 3.00 + 0.15 \bullet (20 - L) & ; \quad L < 15 \quad \text{m} \\ \xi = 1.50 + 0.45 \bullet (20 - L) & ; \quad 15\text{m} \leq L < 20\text{m} \\ \xi = 1.50 & ; \quad L \geq 20 \quad \text{m} \end{cases} \tag{5}$$

6.4. Normative recommendations for the "prestressed concrete" bridge type

When disregarding non-resonant scenarios, the overall lower bound of damping for *"prestressed concrete"* bridges remains above the current normative curve. Additionally, ERRI D214/RP3 [9] does not clearly distinguish between prestressed and reinforced concrete bridges, as no specific damping values or curves are assigned to the former. Finally, although the values provided by NR were not obtained using the controlled procedure described in in Section 3, they may still serve as informative evidence supporting the observation of higher damping in this bridge category. Hence, a revision is justified by merging the *"prestressed concrete"* category with the existing *"filler beam and reinforced concrete"* family, allowing a 0.5% increase in damping without conflicting with the observed lower bounds.

The only exception stands for the Swedish Enköpingsvägen bridge (L = 20.0 m) and Gesällgatan North (L = 30.6 m), highlighted in Fig. 21, but as mentioned in Section 5.4, the former is a clear outlier, while the latter presents a minimum damping ratio of ξ_1 = 1.38%, which is very close to 1.5%. Moreover, all Swedish bridges, including those in the reinforced concrete family, exhibited generally lower damping, likely due to their atypical specific structural configuration with over-sails and

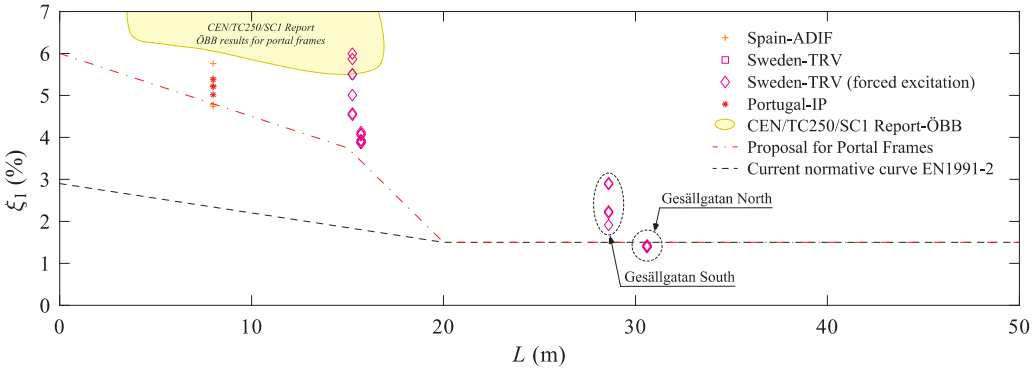

Fig. 20. Newly proposed curve for the "portal frame" bridge category and its comparison with the current stipulated curve in EN 1991–2 [12] for the "filler beam and reinforced concrete" type.

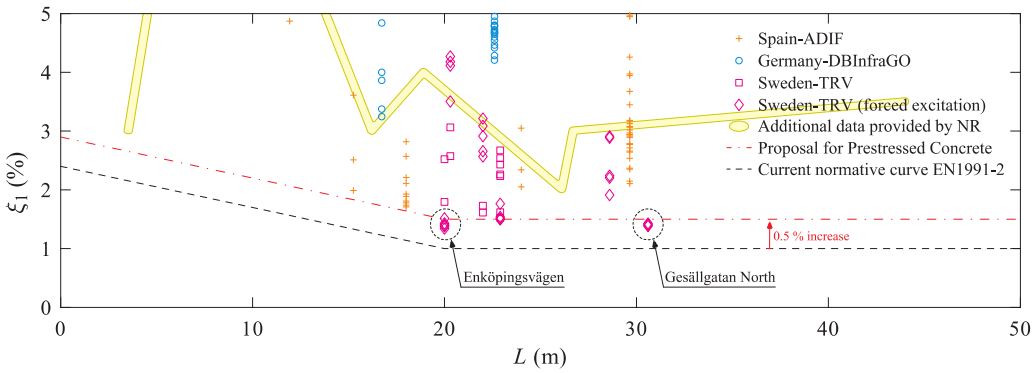

Fig. 21. Newly proposed curve for the "prestressed concrete" bridge category and its comparison with the current stipulated curve in EN 1991–2 [12] for the this type.

pot-bearing supports, which should not constrain the normative proposal. Therefore, the proposed damping curve shown in Fig. 21 excludes such atypical cases and follows the same function currently defined for reinforced concrete bridges.

6.5. Normative recommendations for the "steel-concrete composite" bridge type

Steel–concrete composite bridges are currently grouped with steel bridges in EN 1991–2 [12], sharing the same lower damping bound of 0.5% for spans above 20 m. However, due to their greater mass from the concrete slab, composite bridges typically exhibit higher damping. For instance, BadOldesloe ($L = 30.1$ m) and Banafjällsån ($L = 42.0$ m) weigh approximately 13 t/m and 17 t/m, respectively, while comparable steel bridges such as Boppard ($L = 31.8$ m) and Duisburg ($L = 30.2$ m) weigh only 9 t/m and 6 t/m (see Appendix A). Considering the data in Fig. 18 and the justification of deviations in both this study and ERRI D214/RP3 [9] detailed in Section 5.4, a revision is proposed separating composite bridges from the steel family. The revised curve retains the current values for spans below 20 m and increases the damping from 0.5% to 1.0% for larger spans, introducing a smooth transition between 15 m $\leq L \leq$ 20 m to avoid discontinuities. The piecewise function defining the damping ratio ξ, as function of the span L depicted in Fig. 22 is given by:

$$\begin{cases} \xi = 0.50 + 0.125 \bullet (20 - L) & ; \quad L < 15 \quad \text{m} \\ \xi = 1.00 + 0.025 \bullet (20 - L) & ; \quad 15\text{m} \leq L < 20\text{m} \\ \xi = 1.00 & ; \quad L \geq 20 \quad \text{m} \end{cases} \tag{6}$$

By observing Fig. 22, for spans below 20 m, a few French bridges still fall slightly below the current curve. However, as in other bridge families, lowering the normative line is not justified. For longer spans, as discussed in Section 5.4, apart from the French bridges with inclined lateral girders connected at the bottom by transverse steel beams encased in concrete (highlighted in Fig. 22), which exhibit lower damping likely due to their reduced mass, the overall lower bound generally follows the proposed normative curve. Nevertheless, further studies assessing the steel-to-concrete ratio and its influence on global bending behaviour are recommended to better define exceptions among composite bridges that may not be encompassed within this proposal. Moreover, additional tests should be carried out to better distinguish which composite bridges may exhibit higher damping ratios and which may not.

To further support this recommendation, the composite bridges analysed in ERRI D214/RP3 [9] are also included in Fig. 22. Vieux Briollay, with damping levels ranging from 0.57% to 0.90%, is the only bridge that does not fully meet the 1% proposal and therefore does not constrain the overall recommendation.

6.6. Normative recommendations for the "steel" bridge type

For the *"steel"* bridge type, the lower damping bound after excluding non-resonant cases agrees with the current EN 1991–2 [12] curve (see Fig. 19). No significant deviations were found, thus, since the results are consistent with those reported by the ERRI D214 committee, there is no engineering basis to revise the current normative curve. However, as noted for *"filler-beam and reinforced concrete"* bridges, forced-excitation tests are advised to verify whether higher vibration amplitudes could yield increased damping.

7. Conclusions and further work

The main aim of this study was to improve the characterisation of damping in railway bridges, supporting an evidence-based revision of EN 1991–2 [12]. Using over 1150 acceleration records from 89 European bridges within the InBridge4EU project, revised damping curves

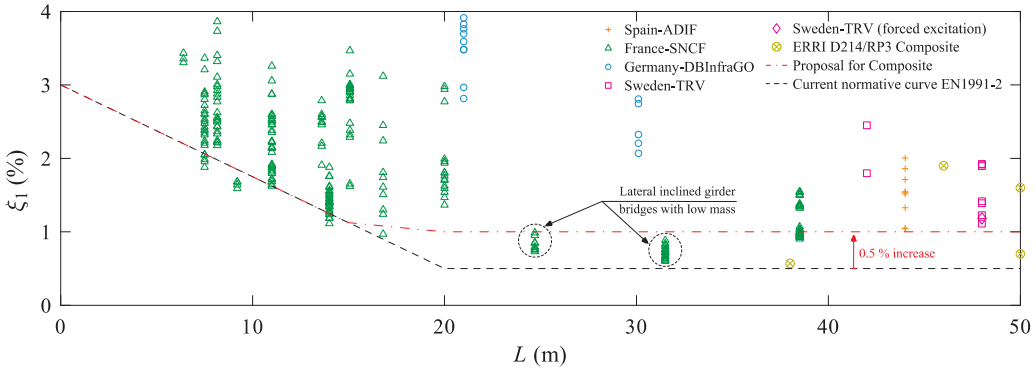

Fig. 22. Newly proposed curve for the "steel-concrete composite" bridge category and its comparison with the current stipulated curve in EN 1991–2 [12] for the "steel and composite" type.

and new bridge typologies are proposed, providing a more accurate basis for assessing existing structures and reducing conservatism in current design values. These results strengthen future code provisions and promote a more consistent assessment of bridge dynamics across the European railway network. Hence, the following conclusions can be drawn from this work:

- The two algorithms for damping estimation, MCO and SSI-COV, were benchmarked against simulated and real bridge responses, showing overall satisfactory agreement.
- Analysis of 1150 records showed no significant correlation between response amplitude and damping, likely because the amplitude variations were insufficient to clearly differentiate the results, and thus had no influence on the proposed normative recommendations.
- Statistical analysis using Austrian railway recommendations [34] proved overly conservative due to scatter, thus, the lower bounds of measured damping values were used for normative recommendations.
- Near-resonant scenarios were identified by isolating the first vertical bending mode, improving on ERRI D214 by allowing abnormal or misleading low values to be critically assessed. Key findings include:

  i) *"Filler beam and reinforced concrete"* bridges align with the current curve.
  ii) When non-near-resonant scenarios are disregarded, *"prestressed concrete"* bridges show higher lower bounds, potentially justifying enhanced damping.
  iii) *"Portal frame"* bridges may represent a new bridge family with higher damping.
  iv) *"Steel–concrete composite"* bridge family could be separated from steel bridges due to generally higher mass and damping, while low-mass outliers should be excluded. ERRI D214 results were also analysed, revealing sound scientific rationale supporting some of the lower damping values estimated at the time. For steel bridges, damping remains aligned with the current normative curve.

- In light of the above, this study provides the first proposal since the 1990s for a revision of the damping curves, which can be summarized by the following recommendations:

  i) Keep the *"filler beam and reinforced concrete"* curve unchanged.
  ii) Merge *"prestressed concrete"* with *"reinforced concrete and filler-beam"* into a single bridge family.
  iii) Define a new *"portal frame"* bridge category.
  iv) Split the *"steel and composite"* family into *"steel"* (existing curve) and *"steel–concrete composite"* with higher damping for longer spans ($L > 20$ m).

The formulation of normative recommendations represents an ongoing effort that extends beyond the results presented in this article. In parallel with the technical developments, the integration of these proposals into a future revision of EN1991–2 is already underway through the structured interactions of the InBridge4EU project with ERA and CEN, ensuring that the underlying evidence is progressively channelled into the relevant Eurocode working groups

Future work should tackle the main limitations of this work, namely to assess higher global modes, conduct forced-excitation tests to reduce scatter, perform a comprehensive analysis of the influence of the free decay segment definition in the damping estimations and refine criteria for the new composite bridge family that account for the steel-to-concrete ratio and its contribution to global bending.

Declaration of Competing Interest

The authors declare that they have no known competing financial interests or personal relationships that could have appeared to influence the work reported in this paper.

Acknowledgements

- Funded by the European Union. Views and opinion expressed are however those of the author(s) only and do not necessarily reflect those of the European Union or the Europe's Rail Joint Undertaking. Neither the European Union nor the granting authority can be held responsible for them. The project InBridge4EU (GA: 101121765) is supported by the Europe's Rail Joint Undertaking and its members.
- The authors would like to acknowledge the European infrastructure managers, namely ADIF, DB InfraGO, Infraestruturas de Portugal, SNCF Réseau and Trafikverket, for providing dynamic test data and for supporting the authors and members of the InBridge4EU consortium in carrying out part of these tests. The authors also acknowledge Ian Bucknall (Network Rail) and Günther Grunert (CEN/TC250/SC1, data from ÖBB) for providing additional indicative data from prestressed concrete bridges in the UK and portal frames in Austria, respectively.
- Also financially supported by Funding UID/04708 of CONSTRUCT - Instituto de I&D em Estruturas e Construções - funded by FCT, I.P./ MCTES through the national funds and by the Stimulus of Scientific Employment, Individual Support (CEECIND) - 5th Edition provided by FCT – Fundação para a Ciência e Tecnologia (Grant No. 2022.00628).

Appendix A. Supporting information

Supplementary data associated with this article can be found in the online version at doi:10.1016/j.engstruct.2026.122666.

Data availability

Bridge description available in the Appendix A as supplementary material. Time-series used to evaluate damping can be made available on request.

References

[1] Stollwitzer A, Fink J, Malik T. Experimental analysis of damping mechanisms in ballasted track on single-track railway bridges. Eng Struct 2020;220:110982. https://doi.org/10.1016/j.engstruct.2020.110982.
[2] Brunetti M, Ciambella J, Evangelista L, Lofrano E, Paolone A, Vittozzi A. Experimental results in damping evaluation of a high-speed railway bridge. Procedia Eng EURODYN 2017 - 10th Int Conf Struct Dyn 2017;199:3015–20.
[3] Ticona Melo L, Malveiro J, Ribeiro D, Calçada R, Bittencourt T. Dynamic analysis of the train-bridge system considering the non-linear behaviour of the track-deck interface (p.) Eng Struct 2020:1–21. https://doi.org/10.1016/j.engstruct.2020.110980.
[4] Stollwitzer A, Bettinelli L, Fink J. The longitudinal track-bridge interaction of ballasted track in railway bridges: Experimental determination of dynamic stiffness and damping characteristics. Eng Struct 2023;274:115115. https://doi.org/10.1016/j.engstruct.2022.115115.
[5] Malveiro J, Ribeiro D, Sousa C, Calçada R. Model updating of a dynamic model of a composite steel-concrete railway viaduct based on experimental tests. Eng Struct 2018;164:40–52. https://doi.org/10.1016/j.engstruct.2018.02.057.
[6] Galvín P, Romero A, Moliner E, De Roeck G, Martínez-Rodrigo MD. On the dynamic characterisation of railway bridges through experimental testing. Eng Struct 2021;226:111261. https://doi.org/10.1016/j.engstruct.2020.111261.
[7] Zangeneh A, Svedholm C, Andersson A, Pacoste C, Karoumi R. Identification of soil-structure interaction effect in a portal frame railway bridge through full-scale dynamic testing. Eng Struct 2018;159:299–309. https://doi.org/10.1016/j.engstruct.2018.01.014.
[8] Reiterer M, Lachinger S, Fink J, Bruschetini-Ambro SZ. Ermittlung der dynamischen Kennwerte von Eisenbahnbrücken unter Anwendung von unterschiedlichen Schwingungsanregungsmethoden. Bauingenieur 2017;92(10):2–13. https://doi.org/10.37544/0005-6650-2017-10-24.
[9] ERRI D214/RP3. Rail bridges for speeds > 200 km/h: Recommendations for calculating damping in rail bridge decks. Utrecht: European Rail Research Institute; 1999.

[10] Silva A, Ribeiro D, Montenegro PA, Ferreira G, Andersson A, Zangeneh A, Karoumi R, Calçada R. New Contributions for Damping Assessment on Filler-Beam Railway Bridges Framed on In2Track EU Projects. Appl Sci 2023;13:2636. https://doi.org/10.3390/app13042636.
[11] Qu C, Tu G, Gao F, Sun L, Pan S, D C. Review of bridge structure damping model and identification method. Sustainability 2024;16:9410. https://doi.org/10.3390/su16219410.
[12] EN 1991-2. Eurocode 1 - Actions on structures - Part 2: Traffic loads on bridges and other civil engineering works. Brussels: European Committee for Standardization (CEN); 2023.
[13] EN 1991-2. Eurocode 1 - Actions on structures - Part 2: Traffic loads on bridges. Brussels: European Committee for Standardization (CEN); 2003.
[14] Andersson, A., R. Allahvirdizadeh, A. Albright, P.A. Montenegro, G. Ferreira, M. Peixer, P. Museros, R. Karoumi, and R. Calçada. *Deliverable D5.6 – Performed high-speed low-cost bridges IN2TRACK3 demonstrators. Project In2Track3 - Research into optimised and future railway infrastructure.* 2022 Available from: ⟨https://projects.shift2rail.org/s2r_ip3_n.aspx?p=IN2TRACK3⟩.
[15] Gattulli V, Lofrano E, Paolone A, Potenza F. Measured properties of structural damping in railway bridges. J Civ Struct Health Monit 2019;9:639–53. https://doi.org/10.1007/s13349-019-00358-3.
[16] Stollwitzer A, Bettinelli L, Loidl S, Schellander J, Vospernig M, Fink J. Novel evaluation methods for data-based determination of damping factors in the frequency and time domains with application on railway bridges (in press.) Railw Eng Sci 2025. https://doi.org/10.1007/s40534-024-00373-1.
[17] Stollwitzer A, Loidl S, Bettinelli L, Fink J. Approach for redefining the damping factor of railway bridges with ballast superstructure: model calibration and guidelines for practical application (in press.) Railw Eng Sci 2025. https://doi.org/10.1007/s40534-025-00387-3.
[18] Glatz B, Fink J. A redesigned approach to the additional damping method in the dynamic analysis of simply supported railway bridges. Eng Struct 2021;241:112415. https://doi.org/10.1016/j.engstruct.2021.112415.
[19] Stoura CD, Dimitrakopoulos EG. Additional damping effect on bridges because of vehicle-bridge interaction. J Sound Vib 2020;476:115294. https://doi.org/10.1016/j.jsv.2020.115294.
[20] Yau JD, Martínez-Rodrigo MD, Doménech A. An equivalent additional damping approach to assess vehicle-bridge interaction for train-induced vibration of short-span railway bridges. Eng Struct 2019;188:469–79. https://doi.org/10.1016/j.engstruct.2019.01.144.
[21] ERA Technical Note. *ERA1193-TD-01-2022 - ERA technical note on work needed for closing TSI open points on bridge dynamics*. 2022; European Union Agency for Railways (ERA); Valenciennes; Available from: ⟨https://rail-research.europa.eu/wp-content/uploads/2022/09/ERA1193-TD-01-2022_ERA-Technical-Note-Bridge-Dynamics.pdf⟩.
[22] InBridge4EU. *Enhanced Interfaces and train categories FOR dynamic compatibility assessment of European railway BRIDGEs.* 2025 2024]; Available from: ⟨https://inbridge4eu.eu/project/⟩.
[23] MATLAB®. 2023a, Natick, MA, USA: Release R2023a, The MathWorks Inc.
[24] Vandekerckhove, J. and R. Oldenhuis. *GODLIKE (Global Optimum Determination by Linking and Interchanging Kindred Evaluators) - A robust single-& multi-objective optimizer*. 2009 2024]; Available from: ⟨https://www.mathworks.com/matlabcentral/fileexchange/24838-godlike-a-robust-single-multi-objective-optimizer⟩.
[25] Peeters B, De Roeck G. Reference-Based Stochastic Subspace Identification for output-only modal analysis. Mech Syst Signal Process 1999;13(6):855–78. https://doi.org/10.1006/mssp.1999.1249.
[26] Magalhães F, Cunha A. Explaining operational modal analysis with data from an arch bridge. Mech Syst Signal Process 2011;25(5):1431–50. https://doi.org/10.1016/j.ymssp.2010.08.001.
[27] Pimenta F, Pedrelli VL, Vanelli T, Magalhães F. On the effect of nonlinear damping sources in output-only identification methods applied to floating wind turbines. Energies 2024;17:1671. https://doi.org/10.3390/en17071671.
[28] Magalhães F. Operational modal analysis for testing and monitoring of bridges and special structures. Porto, Portugal: Faculty of Engineering of the University of Porto; 2010.
[29] Albright A, Battini JM, Andersson A. Dynamic soil-structure interaction of a single-span railway bridge, forced vibration testing and simulation. Struct Infrastruct Eng 2025;21(1):39–48. https://doi.org/10.1080/15732479.2023.2184395.
[30] Ozdemir AA, Gumussoy S. Transfer Function Estimation in System Identification Toolbox via Vector Fitting. IFAC-Pap 2017;50(1):6232–7. https://doi.org/10.1016/j.ifacol.2017.08.1026.
[31] Tehrani SA, Andersson A, Zanganeh A, Battini J-M. Dynamic soil–structure interaction of a three-span railway bridge subject to high-speed train passage. Eng Struct 2024;301:117296. https://doi.org/10.1016/j.engstruct.2023.117296.
[32] Saramago G, Montenero PA, Ribeiro D, Silva A, Santos S, Calçada R. Experimental Validation of a Double-Deck Track-Bridge System under Railway Traffic. Sustainability 2020;14:5794. https://doi.org/10.3390/su14105794.
[33] Montenegro PA, Calçada R. Wheel–rail contact model for railway vehicle–structure interaction applications: development and validation. Railw Eng Sci 2023;31(3):181–206. https://doi.org/10.1007/s40534-023-00306-4.
[34] ÖBB-Regelwerk 08.01.05. *Dynamische Messung von Eisenbahnbrücken*. 2023; ÖBB-Infrastruktur AG; Wien.
[35] EN 1990-Annex D. *Eurocode - Basis of structural and geotechnical design - Annex D: Design assisted by testing*. Brussels: European Committee for Standardization (CEN); 2023.
[36] EN 1990-Annex A2. *Eurocode - Basis of structural and geotechnical design - Annex A.2: Application for bridges.*. Brussels: European Committee for Standardization (CEN); 2023.
[37] Zangeneh A. Dynamic soil-structure interaction analysis of high-speed railway bridges. Stockholm, Sweden: KTH Royal Institute of Technology; 2021.
[38] DIBRST. *Dynamic interface between Railway Bridges and Rolling Stock - State of the art report*. 2023; Draft Report, CEN Technical Committee 250 "Structural Eurocodes", Subcommittee SC1 - EN1991-2 (CEN/TC250/SC1); Brussels.